ACCURACY ASSESSMENT OF ADS40 IMAGERY AS A FUNCTION OF FLYING HEIGHT AND OF AERIAL TRIANGULATION STRATEGIES

V. Casella[a], M. Franzini[a], B. Padova[a]

[a] DIET, University of Pavia, via Ferrata,1- 27100 Pavia, Italy - (vittorio.casella, marica.franzini, barbara.padova)@unipv.it

KEY WORDS: Photogrammetry, Digital, Camera, Georeferencing, Adjustment, Accuracy

ABSTRACT:

The paper concerns an in-depth study of the attainable accuracy of Leica ADS40 imagery. The study has been carried out with the Socet-Set and ORIMA programs and takes advantage of the Pavia Test Site, where many artificial and natural, very well measured control points are available. Three flights are considered, having a relative height of approximately 2000, 4000 and 6000 metres. Different configurations are investigated, characterized by the usage of 0, 1, 5 and 12 GCPs. Finally, several adjustment strategies are analyzed: together with the basic adjustment model, the usage of additional parameters (such as datum transformation and re-estimation of IMU misalignments), as well as the camera self-calibration are taken into consideration.

1. INTRODUCTION

Digital aerial cameras are nowadays a concrete reality. They are significantly present in industrial image and map production: this is demonstrated by some projects in which direct digital acquisition has surpassed the analogue one. For example the NAIP Project of the United States Department of Agriculture, which is about the yearly acquisition of a digital colour orthophoto of the whole of the USA with a ground resolution of 1 or 2 metres. On the manufacturers side, it is probable that the production of the traditional analogue cameras will soon be discontinued.

Digital cameras belong to two large families: the frame cameras, in some ways inspired by the analogue ones, and the line cameras, implementing a totally different and new philosophy. The Leica ADS40 camera is the most important representative of the second family. It is already largely used in production and, to give just a couple of examples, some States of the USA were completely surveyed with it in the NAIP Project, with great customer satisfaction (Welter, 2004). In Italy, the Compagnia Generale Ripreseaeree (CGR in the following) uses two ADS40 cameras for the TerraItaly program, concerning the production of the 0.5 metre colour orthophotos of the complete Italian territory and of the 0.13 metre orthos of more than 150 Italian cities.

Nevertheless, some work still has to be done on the research side, on digital cameras, about the attainable accuracy, the theory of errors (accuracy as a function of flying height, of the number of the images involved in the measurement, etc) and the camera model to be used. Another goal which still has to be reached is the availability of a sufficiently large case study.

The present paper concerns three flights acquired above Pavia in the year 2004, at the relative heights of 2000, 4000 and 6000 metres. The flights were realized by a plane of CGR, equipped with a ADS40 camera. The images were acquired from the Pavia Test Site (PTS in the following), a facility created and maintained by the University of Pavia, provided with many artificial and natural ground control points.

The analysis carried out is about the attainable accuracy as a function of several parameters: the flying height, the number of the GCPs used in the aerial triangulation, the camera model adopted.

Regarding the last item, several options are available and it is very interesting to compare their performances. First of all, the basic camera model, illustrated in (Hinsken et al., 2002), can be used: it mainly assumes the CCD lines are perfectly linear, planar and orthogonal to the flying direction; the centres of the CCD lines are supposed to belong to the line parallel to the flying direction and passing through the principal point. Furthermore, additional external parameters can be estimated, such as a datum transformation between the reference system where the stereoplotted coordinates are determined and a given reference system or the misalignment between reference system of the IMU and the camera's one. The last step is camera self-calibration, whose goal is to take into account deviations of the camera structure from the ideal model: inclination of CCD lines, offsets between the ideal and real positions of their centres and so on.

2. THE TEST SITE AND THE FLIGHTS CONSIDERED

2.1 The Pavia Test Site

PTS has many relevant features which have been developed over the last years, according to the needs of the ongoing research projects. There are features devoted to photogrammetric studies: 186 artificial control points (AGCPs), represented by white squares having a size of 35cm painted on the pavement, and 56 natural control points (NGCPs).

In order to support studies concerning ADS40 imagery, 50 larger artificial markers were added, having a size of 60 cm, called BAGCPs (Big AGCPs). More recently, after the execution of the flights considered in this paper, 70 additional BAGCPs were finally added.

The AGCPs, the NGCPs and the first 50 BAGCPs homogeneously cover the whole PTS, which is 6 x 4.5 km wide. The recently added 70 BAGCPs cover a larger area. The distribution of the BAGCPs used in the present paper, the initial 50, is shown in Figure 4, Figure 5 and Figure 6, projected on the background of the 1:10000 raster map of Pavia.

The size of the markers has been carefully tuned in order to have a satisfactory visibility on all the considered images. The BAGCP markers are clearly visible on the 2000m and 4000m blocks, but still detectable on the 6000m block, as Figure 1, Figure 2 and Figure 3 show.

Figure 1. Visibility on the 2000m block

Figure 2. Visibility on the 4000m block

Figure 3. Visibility on the 6000m block

All the GCPs have been measured with GPS in the fast static mode, using three fixed receivers, set up on vertices of Pavia's GPS network, forming an equilateral triangle. The relative redundancy of the adjustment is therefore three, and the precision of the adjusted coordinates is very good, as Table 1 shows.

	Min [cm]	**Max** [cm]	**Mean** [cm]	**Std** [cm]
e	0.15	0.53	0.26	0.09
n	0.21	0.96	0.42	0.16
u	0.37	1.52	0.74	0.25

Table 1. Mean statistical parameters of standard deviations σ of the 50 BAGCPs, referred to a local Cartesian coordinate system

2.2 The imagery considered

In August 2004, some ADS40 photogrammetric blocks, with different flying heights (2000, 4000 and 6000 metres), were acquired above PTS by the Italian company CGR. Seven ordinary East-West strips were taken: two for the higher block (6000 m), two for the intermediate one (4000 m) and three for the lower one (2000 m). Their outlines and footprints are shown in Figure 4, Figure 5 and Figure 6.

The BAGCPs have a colour code: the green one is used when just 1 control point is inserted into aerial triangulation; the green point plus the red ones are used when 5 control points are inserted; finally, the red and blue points are taken into consideration when the adjustment is performed with 12 points.

Figure 4. Structure of the 2000m block

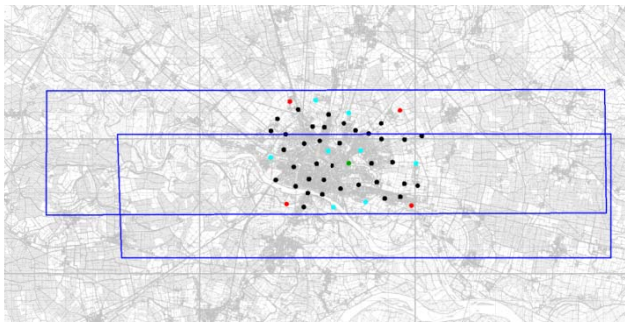

Figure 5. Structure of the 4000m block

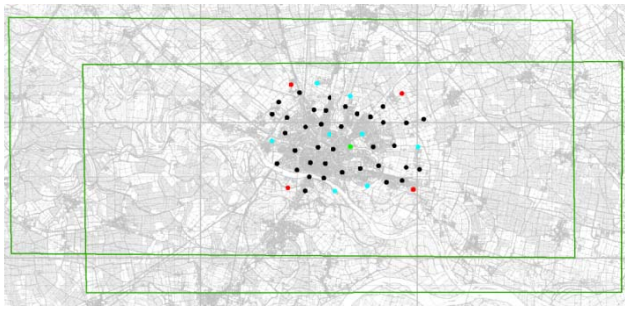

Figure 6. Structure of the 6000m block

2.3 The camera used

The Leica ADS40 camera has just one lens so that the several lines acquired in a certain time are taken from the same position and through the same optics. Furthermore, the camera geometry can be easily modified, simply by moving the CCD arrays on the focal plate. This allowed CGR to customize their first owned camera with respect to the standard structure, originally proposed by Leica, as shown in Figure 7.

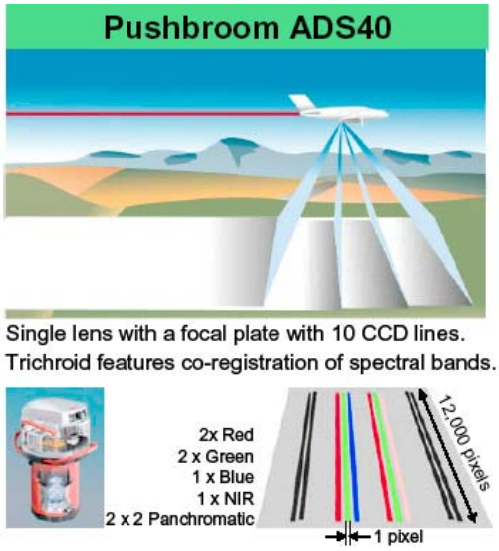

Figure 7. Structure of the ADS40 owned by CGR and used to acquire the studied imagery

The camera focal length is 62.77 mm; the CCD arrays are constituted by 12000 elements of 6.5 microns; the whole sensor width is 78 mm; the nominal FOV is 64°. 10 linear CCD arrays are located on the focal plate of the camera: the forward (28.4° viewing angle) and the backward (14.2° viewing angle) panchromatic arrays are in staggered-array geometry; the 3 RGB

arrays are positioned in the nadir (0° viewing angle) position, while another set of linear CCD arrays (red, green, and near-infrared channels with 14°-18° viewing angle) are in the forward looking angle.

Noticeably, the main feature of the CGR configuration is that the three colour channels are positioned in the nadir position and this allows the acquisition of RGB images without along-track perspective effects: the obtained imagery can be usefully used for orthophoto production.

3. THE MEASUREMENTS PERFORMED ON THE IMAGES

For the analysis described in the paper, only the first 50 BAGCPs were used, because they can be viewed in all the processed images.

The image coordinate measurements of the control points were manually performed at the Geomatics Laboratory of the University of Pavia, with the programs Socet Set and Orima. Tie points were extracted and measured automatically with the APM procedure of Socet Set.

Image measurements were performed once per flight and all the many processing scenarios illustrated in the following come precisely from the same measurements.

In order to insert proper weights into the adjustment, precision of the image coordinates was rigorously assessed. Five BAGCPs were chosen; they are representative of the whole set: some are clearly visible, others not. The sub-images corresponding to the chosen points were extracted from the RGB nadir image and from the panchromatic, forward and backward images, for each flying height. The zoomed 2X and 4X images were calculated using the bilinear method. A large set of fragments was constituted, depending on flying height (2000, 4000 and 6000 metres), zoom factor (2X and 4X), acquisition geometry of the image (nadir, backward and forward), radiometric content (panchromatic and colour).

Successively, three different operators were required to measure each point ten times, in each sub-image. In order to speed up this phase, a special Matlab module was prepared: it shows the operator all the sub-images, one at a time, in a random order and it records the coordinates of the points the operator measures. The module was tuned so that the shape of the cursor and the appearance of the images are similar in the Matlab and Socet Set environments.

	1st operator	2nd operator	3rd operator
2000	0.127	0.120	0.142
4000	0.136	0.127	0.149
6000	0.151	0.130	0.164

Figure 8. Precision of image measurements on the 4X zoomed images

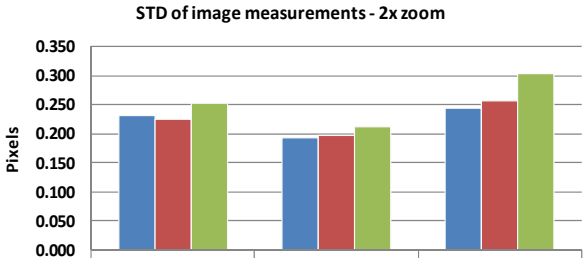

	1st operator	2nd operator	3rd operator
2000	0.230	0.192	0.244
4000	0.224	0.196	0.255
6000	0.251	0.211	0.302

Figure 9. Precision of image measurements on the 2X zoomed images

The analysis of the repeated measurements, which will be exposed in detail in a following paper, led us to two main conclusions, summarized by Figure 8 and Figure 9:

- the 4X zoom ratio gives much better results than the 2X, even if the operators sometimes had the opposite feeling, especially with the lowest flying height;
- on average, the standard deviation of the measurements is below one fifth of a pixel, when 4X zoomed images are observed.

4. THE ANALYSIS PERFORMED

All the data processing was performed with Socet Set 4.4.1, Gpro 2.1 and Orima 6.1.

The basic idea of the assessment performed is to determine by photogrammetry the object coordinates $\mathbf{x}_i^{PHO}$ of n independent check points (ICKs) and to compare them with those given by GPS, $\mathbf{x}_i^{GPS}$, whose accuracy is to the centimetre level; in the considered case, the ICKs are 35. The differences are formed

$$\boldsymbol{\delta}_i = \mathbf{x}_i^{PHO} - \mathbf{x}_i^{GPS} \tag{1}$$

and then single components of the vectors $\boldsymbol{\delta}_i$ are considered

$$\boldsymbol{\delta}_i = \left(\delta_{xi}, \delta_{yi}, \delta_{zi}\right) \tag{2}$$

It is assumed that, for instance, all the n values δ_{xi} are extracted from the same random variable Δ_x, so that the repeated extractions δ_{xi} can be used to estimate the main statistical parameters of Δ_x, which are summarized in the tables shown in the following.

Many different assessment scenarios are considered, as is illustrated in the following, each beginning with an aerial triangulation calculation. The ICKs are inserted into the adjustment as tie points, so that the adjustment gives in output their object coordinates. We state the two following remarks.

- The ICKs are not really independent because they are inserted into the adjustment, so they contribute to it; nevertheless, they are far fewer than the ordinary tie points, which are, in the 2000m flight, around 900, so that the contribution given by ICKs to the adjustment is small and probably negligible.

- The ICK coordinates given by the adjustment can't be treated strictly as extractions from equally-spread random variables, because points are determined by a variable number of rays ranging from 2 to 6. However, the above described procedure is used in most of the papers in the literature and was also adopted by us for the present paper. But in our opinion, a sort of normalization of results should preliminary be performed.

The numerous scenarios considered can be classified according to several parameters.

Flying height. The analysis was performed for the three flights, having relative heights of 2000, 4000 and 6000 metres.

Direct or integrated sensor orientation. Direct georeferencing was assessed, as well as many configurations of integrated sensor orientation. Direct georeferencing was performed through a particular configuration of aerial triangulation: all the observations were given the proper weight, but the data coming from the IMU/GPS system were largely overweighted, in order to force the algorithm to leave them unaltered.

Number of GCPs. When integrated sensor orientation is performed, four scenarios are considered, with 0, 1, 5 and 12 GCPs.
The cases of 5 and 12 correspond to the proper aerial triangulation with control points; the 5 GCP configuration could represent an economic yet hopefully reliable configuration; the other one, with 12 GCPs, is to quantify the gain allowed by a richer configuration.
The other two configurations are more unusual: using just 1 GCP we want to ascertain whether this very minimal control configuration is better than nothing; by performing the aerial triangulation with no GCPs, we want to assess the benefits with respect to direct georeferencing.

Camera model. Two camera models are used, called *basic* and *self*. The first one is described in (Hinsken et al., 2002): it basically assumes that the CCD lines are perfectly linear, planar and orthogonal to the flying direction; beside this, the centres of the CCD lines are supposed to belong to the line parallel to flying direction and passing through the principal point. Finally, it states that the ordinary collinearity equations describe the geometric relationship between object-points and image-points.
The Orima program is however capable of managing more sophisticated camera models. Additional external parameters can be estimated, such as a datum transformation between the stereoplotted coordinates and a given reference system or the misalignment between the reference system of the IMU and the camera's one. Furthermore, camera self-calibration can be performed, whose goal is to take into account deviations of the camera structure from the ideal model: inclination of CCD lines, offsets between ideal and real positions of their centres and so on.

The line structure of the ADS40 camera would require the definition and the implementation of a specific self-calibration mathematical model. As far as the authors know, until this moment, only the model proposed by Gruen and his group tends to this direction. For the time being the Orima program implements the Brown model (Brown, 1976) which was defined for frame cameras; when it is applied to such cameras, the meaning of the additional parameters inserted into the calculation is sufficiently clear; when it is applied to ADS40 imagery instead, the connection between parameters and physical reality is less clear, at least for the authors. Despite this, self-calibration produces a huge gain in results.
During the experiments described in the paper, some guidelines written by the author of Orima, Dr. Hinsken, were followed; they concern the strategies for the choice of additional parameters. The usual, generic criteria of testing significance of additional parameters and avoiding high correlations between them, as far as possible, were also adopted.

In summary, for each flying height, the following scenarios are taken into consideration:

- *DG*: Direct Georeferencing, with no improvement of data coming from IMU/GPS;
- *Basic 0*: the aerial triangulation is performed with the basic model, using no GCPs;
- *Basic 1*: same as above, but with 1 GCP;
- *Basic 5*: same as above, but with 5 GCPs;
- *Basic 12*: same as above, but with 12 GCPs;
- *Self 5*: camera self-calibration is performed during aerial triangulation and 5 GCPs are used;
- *Self 12*: same as above, but with 12 GCPs.

It was decided to perform self-calibration only with 5 GCPs or more, so that the possible scenarios *Self 0* and *Self 1* are not taken into consideration.

5. RESULTS

In the following, results are given for each flying height and for each of the scenarios listed above. For the single components *x*, *y* and *z* of residuals, max, min, mean, standard deviation and rms values are given. They are empirical values, determined by ICKs.

For the sake of clarity, the way the statistical figures are determined is outlined: it may seem pedantic, but often, when reading papers, the exact meaning of the figures shown is uncertain. For the *x* component, for instance

- $mean = m = \frac{1}{n}\sum_{i=1}^{n}\delta_{xi}$
- $std = \sqrt{\frac{1}{n-1}\sum_{i=1}^{n}\left(\delta_{xi} - m\right)^2}$
- $rms = \sqrt{\frac{1}{n}\sum_{i=1}^{n}\delta_{xi}^2}$

Tables are given reporting all the figures: Table 2, Table 3 and 4. Figure 10, Figure 11 and Figure 12 graphically illustrate, instead, the behaviour of the overall accuracy indicator, RMS. In the following, together with the rmsE, rmsN and rmsH figures, already defined, the quantity rmsEN, defined as

$$\mathrm{rmsEN} = \sqrt{\mathrm{rmsE}^2 + \mathrm{rmsN}^2}$$

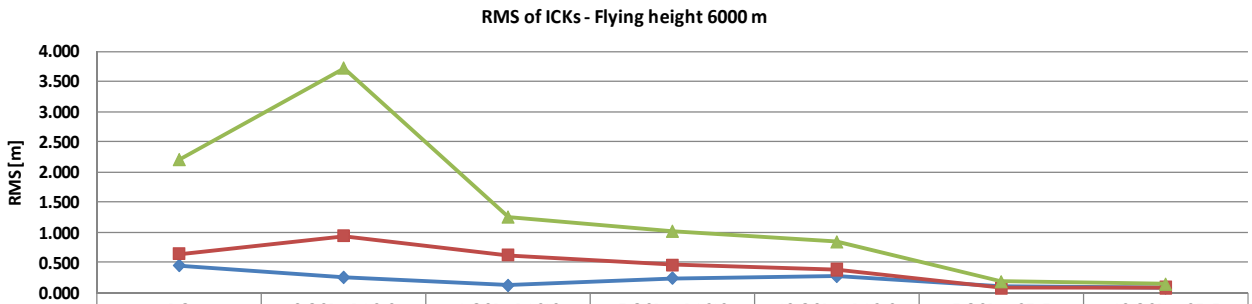

	DG	0 GCP - BASIC	1 GCP - BASIC	5 GCPs - BASIC	12 GCPs - BASIC	5 GCPs - SELF	12 GCPs - SELF
E	0.451	0.255	0.123	0.244	0.271	0.093	0.082
N	0.642	0.935	0.624	0.462	0.382	0.083	0.086
h	2.211	3.727	1.261	1.026	0.850	0.191	0.151

Figure 10. Accuracy figures for 6000m flight

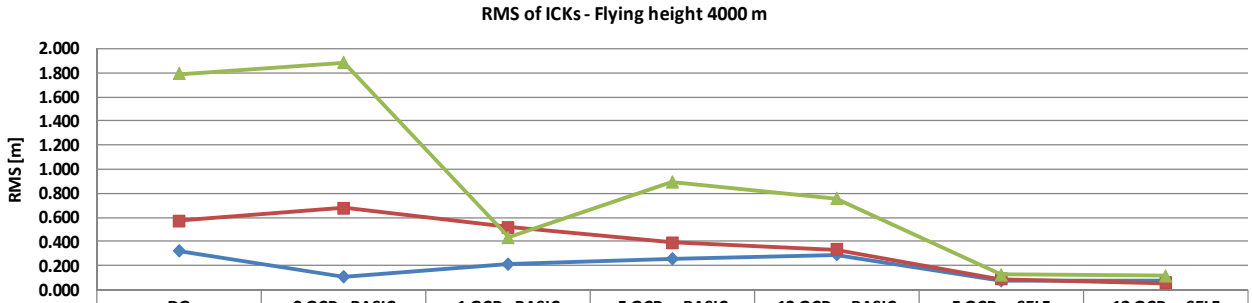

	DG	0 GCP - BASIC	1 GCP - BASIC	5 GCPs - BASIC	12 GCPs - BASIC	5 GCPs - SELF	12 GCPs - SELF
E	0.322	0.107	0.211	0.256	0.291	0.073	0.070
N	0.574	0.677	0.519	0.388	0.331	0.084	0.056
h	1.790	1.881	0.432	0.892	0.756	0.123	0.114

Figure 11. Accuracy figures for 4000m flight

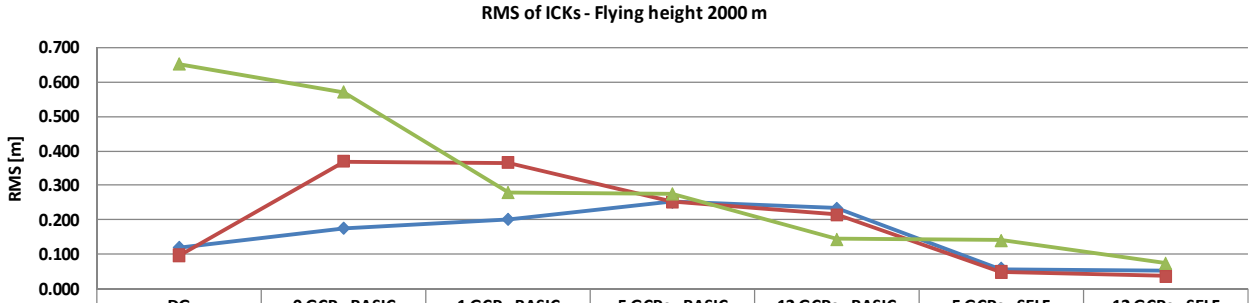

	DG	0 GCP - BASIC	1 GCP - BASIC	5 GCPs - BASIC	12 GCPs - BASIC	5 GCPs - SELF	12 GCPs - SELF
E	0.120	0.176	0.202	0.252	0.234	0.059	0.054
N	0.098	0.369	0.366	0.252	0.215	0.050	0.038
h	0.651	0.570	0.279	0.275	0.143	0.140	0.074

Figure 12. Accuracy figures for 2000m flight

is considered, indicating the overall planimetric error. Furthermore, it is useful to quantify the GSD values at the 6000, 4000 and 2000 metres relative flying height: their approximate values are, respectively, 60, 40 and 20 centimetres.

5.1 Accuracy of 6000m flight (Figure 10)

- In *DG* mode, rmsE and rmsN have the order of magnitude of GSD, while rmsH is more than 4 times larger.
- *Basic 0* case has even worse results: rmsH is significantly greater while rmsEN is comparable.
- Moving right from *Basic 0* rmsEN and rmsH continuously decrease.
- The single error components rmsE and rmsN have a peculiar behaviour: they are more or less the same in *DG* and are significantly split in *Basic 0*, in which rmsN is significantly greater than rmsE; successively, a convergence

process begins, ending in *Basic 12* where the two figures have the same size.

- The best results for *Basic* modes are reached with 12 GCPs and are: rmsE and rmsN equal to 0.5 GSD; rmsH around 1.5 GSD.
- The best results for *Self* modes are reached with 12 GCPs and are: rmsE and rmsN equal to 0.15 GSD; rmsH around 0.25 GSD.
- Self-calibration is needed to reach top quality results.
- The step between *Self 5* and *Self 12* still gives a significant improvement in height.

5.2 Accuracy of 4000m flight (Figure 11)

The analysis is performed following the same schema used for the 6000m flight. As many of the same phenomena are present in all the flights, only the differences between 4000m and 6000m will be highlighted.

- In *DG* mode, rmsE and rmsN have (approximately) the order of magnitude of GSD, while rmsH is more than 4 times larger.
- ***Basic 0* case has comparable results**.
- Moving right from *Basic 0* rmsEN and rmsH continuously decrease. There is the singular exception of *Basic 1*, but we think this is simply a case.
- The single error components rmsE and rmsN diverge in *Basic 0* and converge back in *Basic 12*.
- The best results for *Basic* modes are reached with 12 GCPs (but *Basic 5* is not too far) and are: rmsE and rmsN equal to 0.8 GSD; rmsH around 2 GSD.
- ***Self 5* and *Self 12* perform at the same level**: rmsE and rmsN equal to 0.16 GSD; rmsH around 0.30 GSD.
- Self-calibration is needed to reach top quality results.

5.3 Accuracy of 2000m flight (Figure 12)

- In *DG* mode, rmsE and rmsN are around 0.5 GSD, while rmsH is more than 3 times larger.
- *Basic 0* case has worse results: rmsH is slightly better, but planimetric components are worse.
- Moving right from *Basic 0* rmsEN and rmsH continuously decrease.
- The single error components rmsE and rmsN diverge in *Basic 0* and converge back in *Basic 5*.
- The best results for *Basic* modes are reached with 12 GCPs and are: rmsE and rmsN equal to GSD; rmsH around 0.7 GSD.
- The best results for *Self* modes are reached with 12 GCPs and are: rmsE and rmsN equal to 0.25 GSD; rmsH around 0.30 GSD.
- Self-calibration is needed to reach top quality results.
- The step between *Self 5* and *Self 12* still gives a significant improvement in height.

6000 m			Min [m]	Max [m]	Mean [m]	STD [m]	RMS [m]
DG		E	-0.980	0.233	-0.310	0.327	0.451
		N	-0.616	1.339	0.398	0.504	0.642
		h	-2.725	-1.589	-2.200	0.221	2.211
BASIC	0 GCPs	E	-0.494	0.338	-0.153	0.204	0.255
		N	-0.893	1.970	0.563	0.746	0.935
		h	-4.179	-3.231	-3.721	0.198	3.727
	1 GCPs	E	-0.335	0.251	0.014	0.122	0.123
		N	-0.993	1.391	0.220	0.584	0.624
		h	-1.753	-0.782	-1.245	0.202	1.261
	5 GCPs	E	-0.440	0.572	0.078	0.231	0.244
		N	-0.687	1.014	0.122	0.446	0.462
		h	-1.448	-0.564	-1.009	0.183	1.026
	12 GCPs	E	-0.551	0.604	0.059	0.264	0.271
		N	-0.734	0.674	0.050	0.379	0.382
		h	-1.311	-0.359	-0.829	0.188	0.850
SELF	5 GCPs	E	-0.180	0.183	0.012	0.092	0.093
		N	-0.206	0.209	-0.011	0.082	0.083
		h	-0.320	0.438	0.058	0.182	0.191
	12 GCPs	E	-0.155	0.172	0.010	0.081	0.082
		N	-0.213	0.217	-0.011	0.086	0.086
		h	-0.408	0.220	-0.025	0.149	0.151

Table 2. Complete results for 6000m flight

4000 m			Min [m]	Max [m]	Mean [m]	STD [m]	RMS [m]
DG		E	-0.736	0.254	-0.140	0.290	0.322
		N	-0.486	1.121	0.343	0.461	0.574
		h	-2.169	-1.239	-1.778	0.204	1.790
BASIC	0 GCPs	E	-0.223	0.124	-0.051	0.094	0.107
		N	-0.704	1.528	0.364	0.571	0.677
		h	-2.177	-1.495	-1.874	0.165	1.881
	1 GCPs	E	-0.340	0.423	0.035	0.208	0.211
		N	-0.705	1.175	0.205	0.477	0.519
		h	-0.800	0.003	-0.393	0.180	0.432
	5 GCPs	E	-0.510	0.476	-0.003	0.256	0.256
		N	-0.527	0.785	0.136	0.363	0.388
		h	-1.216	-0.592	-0.881	0.140	0.892
	12 GCPs	E	-0.535	0.570	0.030	0.290	0.291
		N	-0.489	0.668	0.104	0.314	0.331
		h	-1.109	-0.467	-0.742	0.143	0.756
SELF	5 GCPs	E	-0.143	0.186	0.011	0.072	0.073
		N	-0.146	0.161	0.043	0.072	0.084
		h	-0.301	0.180	-0.050	0.112	0.123
	12 GCPs	E	-0.131	0.143	0.005	0.069	0.070
		N	-0.135	0.105	0.008	0.055	0.056
		h	-0.289	0.141	-0.035	0.112	0.114

Table 3. Complete results for 4000m flight

2000 m			Min [m]	Max [m]	Mean [m]	STD [m]	RMS [m]
DG		E	-0.180	0.191	0.012	0.120	0.120
		N	-0.318	0.192	-0.011	0.097	0.098
		h	-0.974	0.052	-0.567	0.321	0.651
BASIC	0 GCPs	E	-0.300	0.343	0.053	0.168	0.176
		N	-0.800	0.731	0.018	0.368	0.369
		h	-0.885	-0.139	-0.539	0.186	0.570
	1 GCPs	E	-0.293	0.390	0.087	0.182	0.202
		N	-0.775	0.737	0.038	0.364	0.366
		h	-0.579	0.206	-0.193	0.201	0.279
	5 GCPs	E	-0.491	0.601	0.062	0.244	0.252
		N	-0.493	0.576	0.019	0.252	0.252
		h	-0.556	-0.027	-0.242	0.132	0.275
	12 GCPs	E	-0.501	0.575	0.014	0.234	0.234
		N	-0.502	0.336	-0.012	0.215	0.215
		h	-0.328	0.080	-0.101	0.101	0.143
SELF	5 GCPs	E	-0.113	0.133	0.023	0.054	0.059
		N	-0.104	0.102	0.024	0.044	0.050
		h	-0.319	0.282	-0.024	0.137	0.140
	12 GCPs	E	-0.153	0.094	-0.012	0.053	0.054
		N	-0.127	0.054	-0.003	0.038	0.038
		h	-0.201	0.116	-0.019	0.072	0.074

Table 4. Complete results for 2000m flight

6. CONCLUSIONS

An in-depth study of the accuracy which is attainable with the Leica ADS40 camera has been carried out. Various parameters have been taken into consideration: flying height, number of GCPs, camera mathematical model.

The overall conclusion is that very good results are attainable, provided that camera self-calibration is performed. Secondly, self-calibration plays a key role and requires, in our opinion, the definition of mathematical models which are specific for line cameras.

It has been underlined that the usage of 12 GCPs, instead of 5, often gives a significant gain: it is reasonable to think that specifically-defined camera models are more efficient and allows for the obtaining of top results with 4/6 GCPs.

7. REFERENCES

Alhamlan, S., Milles, J. P., Walker, A. S., Saks, T. (2004). The influence of ground control points in the triangulation of Leica ADS40 data. *Proceedings of XX Intertanational ISPRS Congress*, on DVD. 12-23 July, Istambul, Turkey.

Brown, D.C. (1976). The Bundle Adjustment - Process and Prospects. *Invited paper to the XIII Congress of ISPRS Commission III.* Helsinki.

Casella, V., Banchini, G. (2004). Verifica della qualità metriche della camera Leica ADS40. *Atti della VIII Conferenza ASITA*, pp. 1983-1988. 14-17 dicembre, Roma.

Casella, V., Franzini, M. (2005). La qualità radiometrica e geometrica della immagini ADS40. *Atti del workshop congiunto AIT e SIFET sul Rilevamento Urbano da Piattaforma Aerea e Satellitare*, on CD-ROM. 1-2 dicembre 2005, Mantova.

Casella, V., Franzini, M., Banchini, G., Basili, D., Gentili, G. (2005). La qualità radiometrica delle immagini ADS40 e la sua influenza sulla precisione di collimazione e di restituzione. *Atti della IX Conferenza ASITA*, pp. 625-628. 15-18 novembre 2005, Catania.

Cramer, M. (2006). The ADS40 Vaihingen/Enz geometric performance test. *ISPR Journal of Photogrammetry and Remote Sensing ,Volume 60,* Issue 6, pp. 363-374.

Hinsken, L., Miller, S., Tempelmann, U., Uebbing, R., Walker, S. (2002). Triangulation of LH Systems'ADS40 imagery using ORIMA GPS/IMU. *Proceedings of ISPRS Commission III Symposium*, on CD. 9-13 September, Graz, Austria.

Kocaman, S., Zhang, L., Gruen, A. (2006). Self-calibrating Triangulation of Airborne Linear Array CCD Cameras. *EuroCOW Workshop*, on CD-ROM. 25-27 january, Castelldefels - Spain.

Welter, J. (2004). USDA Program Goes Digital Over Nebraska. http://gi.leica-geosystems.com/documents/pdf/0405USDAFeature.pdf (accessed 19 apr. 2007)

8. ACKNOWLEDGEMENTS

The research presented in this paper was carried out within the frame of the National Research Project entitled *Analysis, Comparison and Integration of Digital Images Acquired by Aerial and Satellite Platforms*, co-funded by the Italian Ministry of the University for the year 2005 and chaired by prof. Dequal of the Technical University of Torino.

The Compagnia Generale Ripreseaeree, Parma, Italy is gratefully acknowledged for supplying the imagery used.